



Published in final edited form as:

J Med Chem. 2011 April 28; 54(8): 2933–2943. doi:10.1021/jm200022g.

Utilization of Nitrophenylphosphates and Oxime-Based Ligation for the Development of Nanomolar Affinity Inhibitors of the *Yersinia Pestis* Outer Protein H (YopH) Phosphatase, †,§,¶

Medhanit Bahta¹, George T. Lontos², Beverly Dyas³, Sung-Eun Kim¹, Robert G. Ulrich³, David S. Waugh², and Terrence R. Burke Jr.^{1,*}

¹ Chemical Biology Laboratory, Molecular Discovery Program, Center for Cancer Research, National Cancer Institute, National Institutes of Health, NCI-Frederick, Frederick, MD 21702, U.S.A

² Macromolecular Crystallography Laboratory, Center for Cancer Research, National Cancer Institute, National Institutes of Health, NCI-Frederick, Frederick, MD 21702, U.S.A

³ Laboratory of Molecular Immunology, United States Army Medical Research Institute of Infectious Diseases, Frederick, Maryland 21702, U.S.A

Abstract

Our current study reports the first K_M optimization of a library of nitrophenylphosphate-containing substrates for generating an inhibitor lead against the *Yersinia pestis* outer protein phosphatase (YopH). A high activity substrate identified by this method ($K_M = 80 \mu\text{M}$) was converted from a substrate into an inhibitor by replacement of its phosphate group with difluoromethylphosphonic acid and by attachment of an aminooxy handle for further structural optimization by oxime-ligation. A co-crystal structure of this aminooxy-containing platform in complex with YopH allowed the identification of a conserved water molecule proximal to the aminooxy group that was subsequently employed for the design of furanyl-based oxime derivatives. By this process, a potent ($\text{IC}_{50} = 190 \text{ nM}$) and non-promiscuous inhibitor was developed with good YopH selectivity relative to a panel of phosphatases. The inhibitor showed significant inhibition of intracellular *Y. pestis* replication at a non-cytotoxic concentration. The current work presents general approaches to PTP inhibitor development that may be useful beyond YopH.

† A preliminary account of this work has been reported: Bahta *et al.* Application of substrate activity screening in the development of inhibitors of the *Yersinia pestis* protein tyrosine phosphatase, YopH. 238th ACS National Meeting, Washington DC, August 16–20, 2009, MEDI-178.

§ Coordinates and structure factor files have been deposited in the Protein Data Bank with accession code 2Y2F.

¶ Abbreviations: *Y. pestis* (*Yersinia pestis*); YopH (*Yersinia pestis* outer protein H); PTP (Protein tyrosine phosphatase) PTK (Protein tyrosine kinase); *p*NPP (*para*-nitrophenyl phosphate); PTP1B (Protein tyrosine phosphatase 1B); *m*PTPB (*Mycobacterium* protein tyrosine phosphatase B); TFA (trifluoroacetic acid); F₂Pmp (difluorophosphonomethylphenyl); LAR (Leukocyte antigen related); DUSP 14 (Dual specificity phosphatase 14); DUSP 22 (Dual specificity phosphatase 22); BSA (Bovine serum albumin); HEPES (4-(2-hydroxyethyl)-1-piperazineethanesulfonic acid); EDTA (ethylenediaminetetraacetic acid, sodium salt)

* To whom correspondence should be addressed at: Chemical Biology Laboratory, NCI-Frederick, Frederick, P.O. Box B, Bldg. 376 Boyles St., Frederick, MD 21702-1201, Tel: (301) 846-5906; Fax: (301) 846-6033, tburke@helix.nih.gov.

Supporting Information Available: Curves for determination of substrate YopH Michaelis-Menten constants (K_M); YopH inhibition curves for oxime-containing inhibitors **6a–6e**; electron density map for YopH-bound inhibitor **5** and NMR spectra. This material is available free of charge via the Internet at <http://pubs.acs.org>.

Introduction

Maintaining proper levels of tyrosyl phosphorylation through the reversible actions of protein tyrosine kinases (PTKs) and protein tyrosine phosphatases (PTPs) is vital for cellular processes ranging from growth and metabolism to adhesion and differentiation.^{1, 2} Deregulation of PTPs can be linked to diseases, such as diabetes and cancer and accordingly, this class of enzymes represents a new source of potential drug targets.^{3–6} The Gram-negative enterobacterium *Yersinia pestis* (*Y. pestis*) has played an important role in human history as the causative agent of plague,⁷ and more recently it has gained attention due to its possible use as a biological warfare agent. For pathogenicity, *Y. pestis* requires the virulence factor, *Yersinia pestis* outer protein H “YopH,” a highly active PTP.⁸ Accordingly, potent and selective YopH inhibitors could provide a basis for new anti-plague therapeutics. One difficulty encountered in the development of PTP inhibitors is a high incidence of “false positives” that can arise through inhibition of enzyme function by “promiscuous” mechanisms attributable to non-specific factors such as protein aggregation.^{9, 10} It is generally believed that promiscuous inhibitors do not represent valid leads, and avoiding promiscuous mechanisms is an important component of current drug development.¹¹

In theory, avoiding promiscuous behavior could be achieved through the use of substrates as templates for inhibitor design. This is because substrates must interact with their enzyme hosts in non-promiscuous fashions in order for productive catalysis to occur. Employing small non-peptidic arylphosphates to identify potential leads for PTP inhibitor design has been known for some time.^{12–15} However, the explicit application of “substrate activity screening” for the purpose of minimizing misleading promiscuous inhibition has only more recently been proposed by Ellman for protease^{16–20} and PTP targets.²¹ This approach consists of first identifying substrates that exhibit high affinity, structurally enhancing these substrates and then converting the optimized substrates to inhibitors by replacement of their labile phosphoryl groups with suitable non-hydrolyzable phosphoryl mimetics. Additional structural variations can then be performed to further increase inhibitory potency.

In identifying high affinity substrates for the development of PTP inhibitors, advantage can be taken of the hydrolytic action of a PTP on an arylphosphate, which produces both the corresponding phenol and inorganic phosphate. Traditionally, the released inorganic phosphate can be quantified using colorimetric assays that employ phosphomolybdate^{22, 23} or by secondary enzyme assays, including the use of purine nucleotide phosphorylase-mediated phosphate-dependent conversion of 2-amino-6-mercapto-7-methylpurine ribonucleoside to a derivative having an absorbance maximum at 360 nm.²⁴ It is also possible to spectrophotometrically measure the catalytically-produced phenol. A variety of easily detected fluorescence-based substrates are known,²⁵ however these agents would be of little value for the purpose of substrate activity screening and phenols derived from the more structurally-diverse arylphosphates needed for substrate activity screening would typically exhibit very low extinction coefficients.²⁶ An exception to this is found with nitrophenols, which exhibit intense yellow color due to delocalization of the phenolate anionic charge. Because of this property, *para*-nitrophenylphosphate (*p*NPP) has become a ubiquitous substrate for monitoring the activity of phosphatases, including YopH.⁸

In undertaking our current study, we desired to use direct spectrophotometric monitoring of phenol reaction products. For this purpose, we employed substrates (**2**) derived from either *ortho*- or *para*-nitrophenols (**1**, Figure 1). These compounds allowed the simple monitoring (absorbance at λ_{405} nm) of yellow color resulting from the enzyme-catalyzed phosphoryl hydrolysis. Our utilization of nitrophenylphosphates represents the first systematic application of this structural class for PTP substrate optimization.

Once an inhibitor platform has been identified through a substrate activity approach, enhancement of affinity can be undertaken by introducing additional functionality intended to interact with sites proximal to the catalytic cavity.²⁷⁻³³ A distinctive feature of the methodology in our current report is its incorporation of aminooxy functionality into the lead inhibitor platform (**3**) and the use of this handle for oxime-based derivatization (**4**, Figure 1). Functional group ligation by means of oxime bond formation can be considered to be a form of “click chemistry”³⁴ that we³⁵⁻³⁸ and others³⁹⁻⁴² have shown can be highly useful for the facile generation of compound libraries. In the case of PTPs, azide-alkyne Huisgen cycloaddition click reactions have been used previously for the rapid assembly of bidentate libraries targeting protein tyrosine phosphatase 1B (PTP1B) and *Mycobacterium* protein-tyrosine phosphatase B (mPTPB).⁴³⁻⁴⁵ However, a potential limitation of this type of click chemistry is the requirement for high throughput syntheses of azide-containing libraries of reactants.⁴⁶ In contrast, oxime-based click chemistry is advantageous because it can be conducted using commercially available aldehydes and reaction products can be directly evaluated biologically without purification. As reported in our current paper, nitrophenylphosphate-based substrate activity screening used in combination with oxime ligation proved to be highly a successful approach that resulted in the development of a non-promiscuous YopH inhibitor exhibiting a nanomolar IC₅₀ value.

Results and Discussion

Nitrophenylphosphate Substrates

A total of 48 *ortho* and *para* - nitrophenylphosphate-containing substrates (**2**) were prepared by phosphorylation (reaction with HPO₃(Bn)₂) of either commercially available or synthetic nitrophenols, followed by TFA-mediated cleavage of the resulting benzyl protecting groups. The YopH affinities of these substrates were determined using an *in vitro* assay that measured substrate turnover by monitoring the yellow color arising from the reaction product nitrophenols.⁸ Color interference arising from sources other than the nitrophenol products did not prove to be problematic. Assay results for a subset of 11 selected substrates (**2a** – **2k**, Table 1) show that the 3-aminooxymethyl-containing substrate **2e** exhibited a 3.5 - fold decrease in its Michaelis-Menten constant ($K_M = 170 \mu\text{M}$), relative to *p*NPP ($K_M = 600 \mu\text{M}$), while *p*-phenyl-*o*-nitrophenylphosphate (**2j**) showed an approximate 4 - fold decrease in its K_M value (150 μM). The lowest K_M value was obtained with *m*-phenyl-*p*-nitrophenylphosphate (**2k**, $K_M = 80 \mu\text{M}$), which showed an approximate 7.5 - fold decrease relative to reference *p*NPP.

Lead Inhibitor Platform 5

When using substrates as structural models for inhibitor design, the interpretation of data from the substrate enzyme assays can be an important factor. In the current study, K_M values were used to indicate substrate affinity. Previous comparisons of K_M and k_{cat}/K_M values for small molecule non-peptidyl aryl substrates have shown that K_M values more closely reflect IC₅₀ and K_i values than do k_{cat}/K_M ratios.^{12-14, 21} Based on this consideration, substrate **2k** was selected for conversion to an inhibitor because of its low K_M value.

In the conversion of a PTP substrate to an inhibitor, the choice of phosphoryl mimetic can have a dramatic effect on the resulting inhibitory potency.²¹ In our current work α,α -difluoromethylphosphonic acid⁴⁷ was used as a phosphoryl replacement, since it is isosteric with the parent phosphate group and it has been shown to be one of the highest affinity phosphoryl replacements in PTP contexts (Scheme 1).^{48, 49} A further consideration deals with the fate of the nitro-functionality, since its role as a chromophore is no longer needed. Although an example has been reported where protein hydrogen bonding exists for the nitro group of a YopH-bound inhibitor,⁵⁰ in the current work the nitro-functionality was removed

at this stage. The transformation of **2k** to the inhibitor platform **5** was completed by introduction of an aminoxy handle for use in preparing bidentate inhibitors (**6**) using oxime-based click chemistry (Figure 2).³⁴⁻⁴²

Synthesis of Aminoxy-containing Platform 5

The synthesis of **5** began with the CuBr and zinc promoted coupling reaction of diethyl(bromodifluoromethyl)phosphonate with 3-iodobromobenzene⁵¹ to give the corresponding (difluoromethyl)phosphonic acid diethyl ester product **7** (Scheme 1). Suzuki coupling of **7** with 4-hydroxymethylboronic acid to give the biphenyl product **8** was followed by Mitsunobu reaction with *N*-hydroxyphthalimide and treatment of the resulting phthalimide with hydrazine•hydrate to yield the aminoxy-containing diethylphosphonate **9** (79% yield). Finally, conversion of **9** to platform **5** was achieved through TMSBr-mediated phosphonate deprotection (Scheme 1).⁵² (Insert Scheme 1)

Crystal structure of YopH in Complex with Platform 5

In order to facilitate inhibitor optimization, the X-ray co-crystal structure of **5** bound to YopH was determined. The orientation of the phosphonodifluoromethyl group of **5** within the catalytic pocket was observed to be highly similar to that previously reported for the phosphonodifluoromethylphenylalanyl residue (F₂Pmp) of the hexapeptide, Ac-Asp-Ala-Asp-Glu-F₂Pmp-Leu-amide (PDB code: 1QZ0) (Figure 3A).⁵³ The protein backbones of the two structures are nearly superimposable and in both structures the flexible “WPD loops” (residues 354-356) are held in the “closed” conformation. For both structures the phosphoryl-mimicking difluoromethylphosphonic acid group is coordinated within the conserved (H/V)CX5R(S/T) signature motif “P loop” (residues 404-410) by six hydrogen bonds,⁵⁴⁻⁵⁶ while the guanidine group of R409 forms two salt bridges with two phosphonic acid oxygen atoms and indirect hydrogen bonds with residues Q357, Q450 and Q446 are made through a conserved water residue (designated as “Wa1” for ligand **5** and “cw” in PDB 1QZ0). The 1-phenyl ring of **5** is pivoted about the difluoromethylene carbon so that it is offset, yet within the same plane relative to the F₂Pmp aryl ring in the 1QZ0 structure. This allows the 3-(4'-methylphenyl) moiety of **5** to interact similar to the Leu side chain of the dipeptide unit, F₂Pmp-Leu in the 1QZ0 structure (Figure 3A). The aryl rings of **5** form extensive hydrophobic contacts with residues F229, D231, I232, A405, Q446 and I443, similar to what is observed in the 1QZ0 structure (Figure 3A & 3B and Table 2).

Introduction of Oxime Functionality into 5

In the co-crystal structure the aminoxy amine of **5** forms hydrogen bonds with the side chain carboxyl of D231 and a water molecule (Wa43), which also hydrogen bonds to the D231 residue (Figure 4A). The importance of this latter water is indicated by its presence in the absence of inhibitor (designated as “Wa87” in PDB code 1LYV), suggesting that it could be used for inhibitor design. *In silico* docking studies performed using the co-crystal structure of **5** with the inclusion of Wa43^{57, 58} identified furanyl-based oximes as providing favorable interactions with the D231 residue through the intermediacy of the conserved water (Figure 4B).

Syntheses of a series of furanyl-based oxime inhibitors was performed in DMSO by reacting **5** (24 mM) with a commercially available furanyl aldehydes and AcOH in the ratio (1 : 1 : 2). The oxime products (**6**), which were typically of >90% purity as shown by random HPLC analysis, were used directly for biological evaluation. Inhibitory potencies (IC₅₀ values) were obtained spectrophotometrically in an *in vitro* YopH assay using pNPP as substrate.³⁸

The 3-furanyloxime (**6a**) showed an IC₅₀ value of 3.69 μM, whereas the 2-furanyloxime (**6b**) was approximately 3-fold more potent (IC₅₀ = 1.20 μM) (Table 3). In modeling studies, the furanyl oxygen in **6a** was seen to be at a greater distance from the conserved Wa43 than for **6b**. Therefore **6b** was modified by sequential addition of a 5-methyl group (**6c**, IC₅₀ = 0.91 μM) and then by introducing a hydroxyl group onto this methyl (**6d**, IC₅₀ = 0.73 μM) and finally by oxidation of the 5-hydroxymethyl substituent to a carboxyl group (**6e**, IC₅₀ = 0.19 μM). This sequence of modifications resulted in a 6-fold improvement relative to the parent **6b**. The observed binding enhancement of **6e** was consistent with *in silico* docking studies that showed multiple interactions of its carboxyfuranyl oxime with the conserved Wa43 as well as with the backbone amide proton of R230 (Figure 4C).

Examination of Specificity of 6e

The development of YopH inhibitors is less advanced than for several other phosphatases. For example, while the literature contains numerous reports of nanomolar-affinity PTP1B inhibitors,⁵⁹ there are few examples of YopH inhibitors exhibiting affinities in the submicromolar range.^{30, 60} Additionally, the development of PTP inhibitors is plagued by a high incidence of false positives that are due to nonspecific or promiscuous mechanisms arising from the formation of colloid protein aggregates,^{9, 10, 61, 62} and for some YopH inhibitors the possible roles of promiscuous mechanisms are unclear. The nanomolar IC₅₀ value of **6e** makes it one of the more potent YopH inhibitors reported to date. In order to determine whether promiscuous mechanisms are at work, assays were conducted in the presence and absence of 0.01% TX-100, since it is known that promiscuous inhibition can often be minimized by the addition of such a detergent.⁶² These experiments showed that the inhibitory potency of **6e** is independent of detergent concentration, providing strong evidence that YopH inhibition by **6e** does not arise through promiscuous mechanisms.

It was also of interest to examine possible YopH selectivity of **6e**, since significant structural homology exists among many phosphatases. For this purpose, the inhibitory activity of **6e** was measured against a panel of phosphatases that included the classical tyrosine-specific phosphatases PTP1B and leukocyte antigen related phosphatase (LAR),⁶³ as well as the dual specificity phosphatases 14 and 22⁶⁴ DUSP14, DUSP22 and the Variola phosphatase VH1. In these assays **6e** showed an approximate 17-fold selectivity for YopH relative to PTP1B and greater than 2000-fold selectivity relative to the other phosphatases examined (Table 4).

Evaluation of 6e in Biological Models

A cell-based assay was used to assess toxicity of **6e**. The mouse macrophage line J774 was cultured 40 h with 0.1–100 μM of **6e** and toxicity was measured by cellular ATP content. No toxicity for any compound was observed for **6e** at concentrations below 100 μM (data not shown). Intracellular replication of *Y. pestis* was assessed by a previously described human monocyte infection model.⁶⁵ Primary human monocytes were infected for 12 h with *Y. pestis*, using cell culture media containing 0.1–100 μM inhibitors or control. Specific inhibition of intracellular bacterial growth was observed with 10 μM concentrations of **6e** (Figure 5). An approximately 9-fold decrease in intracellular bacteria resulted from treatment with **6e** compared to a negative control that showed no inhibition of YopH. The positive control gentamycin (10 μM), which targets bacterial ribosomes,⁶⁶ produced nearly complete inhibition of intracellular *Y. pestis* growth.

Conclusions

YopH has proven to be a difficult target for inhibitor development. While there are numerous reports of nanomolar affinity inhibitors against other phosphatases such as PTP1B, submicromolar affinity YopH inhibitors are very few. The current study represents

the first utilization of a library of nitrophenylphosphate-containing substrates for the purposes of lead identification. An attractive feature of this approach is that K_M values can be calculated directly by colorimetric methods based on the enzymatic generation of nitrophenol chromophore-containing reaction products. The current work is also characterized by its use of oxime-based click ligation to optimize a substrate-derived lead. The combination of these two methodologies allowed the identification of a non-promiscuous nanomolar affinity YopH inhibitor exhibiting good PTP selectivity that showed significant inhibition of intracellular *Y. pestis* replication at a non-cytotoxic concentration. The current work provides valuable insights into the development of YopH inhibitors that may have broader applicability in the discovery of inhibitors directed against other phosphatases.

Materials and Methods

General

The following reagents used for YopH enzyme assays were obtained from Sigma-Aldrich: pNPP tablets; 30% BSA solution (protease free); 1.0 M HEPES solution (pH 7.0 – 7.6) and dithiothreitol (DTT). Aqueous ethylenediaminetetraacetic acid, sodium salt EDTA (0.5 M, pH 8.0) was obtained from Invitrogen and 96-well plates were purchased from Costar. All reactions were carried out under argon unless otherwise stated. All solvents were anhydrous and obtained from Sigma-Aldrich. Final products were purified by a high pressure liquid chromatography (HPLC) using a Waters Prep-LC 4000 system and Phenomenex Gemini 10 μ , 110 Å C18 columns (250 \times 21.20 mm 10 micron) at a flow rate of 10 mL/minute (prep. HPLC) with a mobile phase of A = 0.1% aqueous TFA and B = 0.1% TFA in aqueous acetonitrile. Typical gradients were from 10% B to 100% B over 40 minutes with UV monitoring at 220 nm, 254 nm and 280 nm. The purity of final products was determined by analytical HPLC using a Waters Prep-LC 4000 system and Phenomenex Gemini 5 μ , 110 Å C18 columns (250 \times 4.60 mm 5 micron) at a flow rate of 1 mL/minute with a mobile phase of A = 0.1% aqueous TFA and B = 0.1% TFA in aqueous acetonitrile. All final products were found to be \geq 95% pure. NMR spectra were recorded using a Varian 400 MHz spectrometer. Unit mass resolution LC-MS were obtained on synthetic intermediates and high resolution mass spectra (HRMS) were obtained for final products (University of California at Riverside Mass Spectral Facility). Optical densities were measured with Biotek Synergy 2 spectrophotometer at λ_{abs} 405 nm using a kinetic readout for determination of K_M values and absolute readout for determination of IC_{50} values. The PTPse domain of YopH (residues 164-468) was expressed in *Escherichia coli* according to the previously published procedure.⁵³

Recombinant Proteins

The PTPase domain of YopH (residues 164-468) was expressed in *Escherichia coli* and purified as described previously.^{8, 53} as were the Variola major H1 (VH1)⁶⁷ and human DUSP-14 dual specificity phosphatases.⁶⁸ Human DUSP-22, PTP1B and LAR catalytic domains were expressed and purified using generic methodology.⁶⁹

Determination of YopH Michaelis-Menten Constants (K_M) for Nitrophenylphosphates

Total reactions volumes of 100 μ L/well of reaction volume were used in 96 well plates. Buffer was prepared by mixing 25 mM Hepes buffer (pH 7.0 – 7.6), 50 mM NaCl, 2.5 mM EDTA, and 5 mM dithiothreitol (DTT) with 1mM fresh DTT added right before assay run. To each well was added 85 μ L assay buffer, 0.25% BSA (5 μ L) followed by 5 μ L of nitrophenylphosphate substrate in DMSO at dilutions of 1000, 500, 250, 125, 50, 25, 10 and 5 μ M. To the reaction mixtures was then added 5 μ L of YopH in buffer (25 μ g/mL) and hydrolysis of substrate was monitored at 30 seconds intervals over 15 minutes. Michaelis-

Menten constants (K_M values) were determined using non-linear regression with the equation $y = V_{\max}[x/(K_M+x)]$. Values for *p*NPP and synthetic substrates **2a** – **2k** are shown in Table 1. Data curves are provided in the Supporting Information.

Determination of YopH IC₅₀ Values

Total reactions volumes of 100 μ L/well of reaction volume were used in 96 well plates. Buffer was prepared as above. To each well was added 79 μ L of assay buffer, 0.25% BSA (5 μ L) followed by 5 μ L of inhibitors in DMSO at dilutions of 400, 133, 44, 15, 5, 1.67, 0.56, 0.19, 0.063, 0.032 and 0 μ M. To the reaction mixtures was then added 5 μ L of YopH in buffer (25 μ g/mL) followed by 6 μ L of 10 mM *p*NPP buffer and each plate was agitated gently at 25° C for 15 – 20 minutes. Hydrolysis of the substrate was immediately measured. IC₅₀ values were determined by fitting the data with sigmoidal curve generated using the Boltzman equation. A parallel independent assay was performed with 0.01% TritonX-100. Inhibition constants for **6a** – **6e** are provided in Table 3. Data curves are provided in the Supporting Information.

Toxicity Assay

Toxicity of **6e** was assessed with the mouse macrophage line J774 (American Type Culture Collection, Manassas, VA), cultured in Eagle's Minimum Essential Medium supplemented with 4 mM L-glutamine, 4500 mg/L glucose, 1500 mg/L sodium bicarbonate, and 7.5% fetal bovine serum (GIBCO/Invitrogen, Carlsbad, CA). Cells were grown in 96 well (5x10⁵ cells/100 mL), polystyrene plates (opaque bottom; Corning, Lowell, MA), maintained in a 5% CO₂, humid air incubator (37°C). Inhibitor **6e** was dissolved in DMSO to produce a 10 mM stock solution, and then added to cultures by diluting in media to final concentrations of 0.1–100 μ M. A negative control was also used that shows no inhibition of YopH. Culture media for all cells contained a final 1% DMSO, including control wells without chemical compounds. Cell viability was assessed by ATP content 20 and 40 h after treatment, using a commercial kit (ViaLight, Lonza, Basel, Switzerland) and a luminometer (Wallac 1420 Victor; PerkinElmer, Shelton, CT) to measure photon emission.

Intracellular Replication of Bacteria

Primary human monocyte cultures⁶⁵ were used to measure intracellular replication of the plague bacterium. The *Y. pestis* strain CO92 *pgm*–, *pla*–, was previously described.⁷⁰ Colony-isolated bacteria were grown 12 h in heart-infusion broth (HIB; Difco Laboratories, Detroit, MI) supplemented with 0.2% xylose and 2.5 mM CaCl₂. A dilution of the culture was grown (26° C) to mid-log phase, and the bacteria were pelleted by centrifugation (600 \times g) before rinsing with RPMI 1640 medium. Human peripheral blood monocytes (CD14+) were isolated as previously described⁶⁵ and added (2 \times 10⁵/well) to tissue culture plates (96 well, flat bottom; Corning) in 100 μ L RPMI 1640 supplemented with 5% human AB sera (Life Technologies, Carlsbad, CA). The monocytes were incubated (1 h, 37° C) with a 1:1 ratio of *Y. pestis* in a 5% CO₂, humid air incubator (37° C). The wells were pulsed with gentamycin (10 μ g/mL; 20 minutes) and rinsed with warm media to remove remaining extracellular bacteria. The cells were then cultured for 12 h in a 5% CO₂, humid air incubator (37° C) in media (100 μ L RPMI 1640 supplemented with 5% human AB sera) containing 0.1–100 μ M of **6e** or a negative control that shows no inhibition of YopH. As a positive control, gentamycin was added to wells containing no other inhibitors. All cultures contained 1% DMSO by volume. The wells were then gently washed with warm medium, followed by addition of 120 μ L of sterile distilled water to lyse the cells. The cell lysates were serially diluted (1:5) in HIB, and 200 μ L of each dilution was placed into duplicate wells of a culture plate (Honeycomb; Growth Curves USA, Piscataway, NJ) and placed in a growth-monitoring incubator (Bioscreen; Growth Curves USA) with constant agitation (37°

C). Bacterial growth was measured by optical density at 600 nm every 20 minutes for 16 h. The amount of *Y. pestis* was quantified by comparison to a standard curve of bacteria.

X-ray Crystallography

The purified protein was pooled and concentrated by diafiltration to 17.6 mg/mL in 100 mM sodium acetate pH 5.7, 100 mM NaCl, and 1 mM EDTA. Crystals of YopH were obtained with condition D8 (0.1M Buffer System 2 pH 7.5, 0.12 M alcohols, 12.5 % v/v MPD, 12.5% w/v PEG 1000, and 12.5% w/v PEG 3350) from the Molecular Dimensions (Apopka, FL) Morpheus Screen. A 1:1 ratio of protein (17.6 mg/mL) to well solution was used for crystallization at room temperature. Plate-like crystals grew within 3 days. To obtain the protein-inhibitor complex, compound **5** was dissolved in DMSO and added to the crystallization solution to obtain a final concentration of 10 mM (10% DMSO). The crystals were added to the soaking solution and soaked for 48 h at room temperature. Crystals were flash frozen in liquid nitrogen without the need of an additional cryoprotectant.

X-ray diffraction data for the YopH-compound **5** complex were collected at beamline 22-ID of the SER-CAT facilities at the Argonne National Laboratory utilizing remote data collection. Using a 1.0 Å X-ray wavelength, 180 frames of data were collected using an exposure time of 3 seconds and oscillation angle of 1 degree. The X-ray diffraction data were processed with HKL3000.⁷¹ Data collection and refinement statistics are outlined in Table 5. The structure was solved by molecular replacement using the MOLREP program⁷² from the CCP4 suite⁷³ and the coordinates of the previously solved YopH structure (PDB code: 1QZ0) after removing all solvent and ligand atoms. Cross-rotation and translational searches were performed using data up to 3.0 Å followed by rigid-body refinement with REFMAC5.⁷⁴ Iterative rounds of model rebuilding and refinement were performed with COOT⁷⁵ and REFMAC5 and the location of the inhibitor was unambiguously identified using σ_A -weighted $2mF_o-DF_c$ and mF_o-DF_c electron density maps.⁷⁶ The coordinates and refinement restraint files were prepared using the Dundee PRODRG server.⁷⁷ Water molecules were located using COOT and refined with REFMAC5. The refinement was monitored by setting aside 5% of the reflections for calculation of the R-free value.⁷⁸ Model validation was performed using MolProbity.⁷⁹ The electron density map for YopH-bound inhibitor **5** is included in the Supporting Information. The coordinates and structure factor files were deposited in the Protein Data Bank with accession code 2Y2F.

In Silico Studies

Docking of inhibitors **6a** and **6e** onto YopH was done with ICM Chemist Pro[®] software⁵⁷ running on a MacIntosh computer (OSX v10.5.8) using default parameters and procedures.⁵⁸ In summary, modeling started with the X-ray crystal structure of YopH in complex with **5**. The “convert PDB” command was used to convert to native ICM format, with optimization of hydrogens. All H₂O molecules were removed from the enzyme with the exception of the catalytically-conserved water (Wa1) and a conserved water proximal to the ligand aminoxy group (Wa43) (see Figure 4A). A 2-furanyl-based oxime group was added to the aminoxy-amine of **5** and the resulting oxime structure (**6a**) was re-docked using the “re-dock” option under the “Ligand” menu (see Figure 4B). All docking experiments were performed using the standard “re-dock” command, which utilizes a rigid receptor protocol. The docked **6a** was then modified by addition of a carboxyl group to the furanyl 5-position and the resulting structure (**6e**) was re-docked as described above (see Figure 4C).

General Procedure for the Synthesis of Nitrophenylphosphate Substrates (2a – 2k)

To a solution of *ortho*- or *para*-nitrophenol (1.0 mmol) in CH₂Cl₂ (5 mL) was added CCl₄ (5.0 mmol) at -15° C and the reaction mixture was stirred at -15° C (5 – 10 minutes). To

the mixture was added *NN*, -diisopropylethylamine (DIEA) (2.0 mmol) and *NN*, -dimethylaminopyridine (DMAP) (0.1 mmol), then dibenzyl phosphite was added dropwise at -15°C and the mixture was stirred at -15°C (1.5 h). The reaction was quenched by stirring with 0.5 M aqueous KH_2PO_4 (20 mL) at room temperature (5 minutes). The aqueous phase was extracted with EtOAc, and the combined organic extract was dried (MgSO_4) and taken to dryness under reduced pressure. The resulting residue was stirred with a solution TFA : CH_2Cl_2 (1 : 1; 5 mL) for 2 – 3 h, volatiles were removed by evaporation and crude products were subjected to HPLC purification to provide final products in yields of 75% – 100%.

4-(*Tert*-butyl)-2-nitrophenyl Dihydrogen Phosphate (2a)

^1H NMR (400 MHz, CD_3OD): δ 7.86 (d, J = 2.0 Hz, 1H), 7.67 (dd, J = 2.4 Hz, J = 8.8 Hz, 1H), 7.44 (d, J = 8.8 Hz, 1H), 1.31 (s, 9H). ^{13}C NMR (400 MHz, CD_3OD): δ 149.99 (1C), 143.19 (1C), 143.04 (1C), 132.27 (1C), 123.66 (1C), 123.06 (1C), 35.69 (1C), 31.49 (3C). HRMS-ESI (m/z): $[\text{M} - \text{H}]^-$ calcd for $\text{C}_{10}\text{H}_{14}\text{NO}_6\text{P}$, 274.0486; found, 274.0490.

3-(*Tert*-butyl)-4-nitrophenyl Dihydrogen Phosphate (2b)

^1H NMR (400 MHz, CD_3OD): δ 7.42–7.46 (m, 2H), 7.18 (m, 1H), 1.39 (s, 9H). ^{13}C NMR (400 MHz, CD_3OD): δ 154.17 (1C), 149.26 (1C), 144.82 (1C), 126.89 (1C), 121.66 (1C), 119.79 (1C), 35.28 (1C), 29.36 (3C). HRMS-ESI (m/z): $[\text{M} - \text{H}]^-$ calcd for $\text{C}_{10}\text{H}_{14}\text{NO}_6\text{P}$, 274.0486; found, 274.0490.

4-((Aminoxy)methyl)-2-nitrophenyl Dihydrogen Phosphate (2c)

^1H NMR (400 MHz, D_2O): δ 8.09 (d, J = 2.2 Hz, 1H), 7.78 (dd, J = 2.4 Hz, J = 8.8 Hz, 1H), 7.59 (d, J = 8.8 Hz, 1H), 5.09 (s, 2H). HRMS-ESI (m/z): $[\text{M} - \text{H}]^-$ calcd for $\text{C}_7\text{H}_8\text{N}_2\text{O}_7\text{P}$, 263.0075; found, 263.0077.

3-((Aminoxy)methyl)-4-nitrophenyl Dihydrogen Phosphate (2d)

^1H NMR (400 MHz, D_2O): δ 8.27 (d, J = 9.2 Hz, 1H), 7.53 (s, 1H), 7.40 (d, J = 9.2 Hz, 1H), 5.41 (s, 2H). HRMS-ESI (m/z): $[\text{M} - \text{H}]^-$ calcd for $\text{C}_7\text{H}_8\text{N}_2\text{O}_7\text{P}$, 263.0075; found, 263.0067.

3-(((ethylideneamino)oxy)methyl)-4-nitrophenyl Dihydrogen Phosphate (2e)

^1H NMR (400 MHz, CD_3OD): δ 8.16 (d, J = 9.2 Hz, 1H), 7.36 (m, 1H), 7.27 (m, 1H), 6.98 (q, J = 5.6 Hz, 1H), 5.40 (s, 2H), 1.88 (d, J = 5.6 Hz, 3H). HRMS-ESI (m/z): $[\text{M} + \text{H}]^+$ calcd for $\text{C}_9\text{H}_{12}\text{N}_2\text{O}_7\text{P}$, 291.0377; found, 291.0374.

2-Methyl-4-nitrophenyl Dihydrogen Phosphate (2f)

^1H NMR (400 MHz, CD_3OD): δ 8.06 (m, J = 4.0 Hz, 1H), 8.00 (dd, J = 4.0 Hz, J = 8.0 Hz, 1H), 7.42 (d, J = 8.0 Hz, 1H), 2.34 (s, 3H). ^{13}C NMR (400 MHz, CD_3OD): δ 156.26 (1C), 145.43 (1C), 132.75 (1C), 127.32 (1C), 123.68 (1C), 121.33 (1C), 16.65 (1C). HRMS-ESI (m/z): $[\text{M} - \text{H}]^-$ calcd for $\text{C}_7\text{H}_8\text{NO}_6\text{P}$, 232.0016; found, 232.0011.

2-Methyl-6-nitrophenyl Dihydrogen Phosphate (2g)

^1H NMR (400 MHz, CD_3OD): δ 7.67 (dd, J = 1.2 Hz, J = 8.0 Hz, 1H), 7.50 (d, J = 9.5 Hz, 1H), 7.20 (td, J = 1.2 Hz, J = 8.0 Hz, 1H), 2.41 (s, 3H). ^{13}C NMR (400 MHz, CD_3OD): δ 145.15 (1C), 143.43 (1C), 136.75 (1C), 135.56 (1C), 126.02 (1C), 124.10 (1C), 17.04 (1C). HRMS-ESI (m/z): $[\text{M} + \text{H}]^+$ calcd for $\text{C}_7\text{H}_8\text{NO}_6\text{P}$, 234.0162; found, 234.0160.

2-Cyclohexyl-4-nitrophenyl Dihydrogen Phosphate (2h)

Spectral data ^1H NMR (400 MHz, CD_3OD): δ 7.68 (dd, $J = 1.6$ Hz, $J = 8.0$ Hz, 1H), 7.61 (dd, $J = 1.2$ Hz, $J = 8.0$ Hz, 1H), 7.30 (td, $J = 1.2$ Hz, $J = 8.0$ Hz, 1H), 3.09 (m, 1H), 1.75–1.88 (m, 5H), 1.30–1.53 (m, 5H). ^{13}C NMR (400 MHz, CD_3OD): δ 155.29 (1C), 145.93 (1C), 141.78 (1C), 123.91 (1C), 123.41 (1C), 121.50 (1C), 38.59 (1C), 34.19 (2C), 27.90 (2C), 27.20 (1C). HRMS-ESI (m/z): $[\text{M} + \text{H}]^+$ calcd for $\text{C}_{12}\text{H}_{16}\text{NO}_6\text{P}$, 300.0642; found, 300.0642.

2-Cyclohexyl-6-nitrophenyl Dihydrogen Phosphate (2i)

^1H NMR (400 MHz, CD_3OD): δ 8.15 (m, 1H), 8.07 (dd, $J = 2.8$ Hz, $J = 8.8$ Hz, 1H), 7.52 (dd, $J = 1.2$ Hz, $J = 8.8$ Hz, 1H), 3.30 (m, 1H), 1.77–1.90 (m, 5H), 1.32–1.51 (m, 5H). ^{13}C NMR (400 MHz, CD_3OD): δ 145.11 (1C), 144.68 (1C), 142.13 (1C), 133.31 (1C), 126.30 (1C), 123.85 (1C), 38.10 (1C), 34.77 (2C), 27.89 (2C), 27.20 (1C). HRMS-ESI (m/z): $[\text{M} + \text{H}]^+$ calcd for $\text{C}_{12}\text{H}_{16}\text{NO}_6\text{P}$, 300.0642; found, 300.0642.

3-Nitro-[1,1'-biphenyl]-4-yl Dihydrogen Phosphate (2j)

^1H NMR (400 MHz, CD_3OD): δ 8.07 (dd, $J = 0.8$ Hz, $J = 2.4$ Hz, 1H), 7.85 (dd, $J = 2.0$ Hz, $J = 8.4$ Hz, 1H), 7.58–7.60 (m, 3H), 7.41–7.45 (m, 2H), 7.35 (m, 1H). ^{13}C NMR (400 MHz, CD_3OD): δ 155.48 (1C), 144.51 (1C), 139.62 (1C), 139.38 (1C), 130.29 (2C), 129.47 (1C), 128.01 (2C), 124.44 (1C), 124.41 (1C), 124.36 (1C). HRMS-ESI (m/z): $[\text{M} + \text{H}]^+$ calcd for $\text{C}_{12}\text{H}_{11}\text{NO}_6\text{P}$, 296.0319; found, 296.0315.

6-Nitro-[1,1'-biphenyl]-3-yl Dihydrogen Phosphate (2k)

^1H NMR (400 MHz, CD_3OD): δ 7.95 (d, $J = 8.8$ Hz, 1H), 7.40–7.43 (m, 3H), 7.34–7.38 (m, 2H), 7.30–7.32 (m, 3H). ^{13}C NMR (400 MHz, CD_3OD): δ 155.48 (1C), 146.76 (1C), 139.79 (1C), 138.63 (1C), 129.76 (2C), 129.49 (1C), 128.90 (2C), 127.35 (1C), 129.32 (1C), 120.89 (1C). HRMS-ESI (m/z): $[\text{M} + \text{H}]^+$ calcd for $\text{C}_{12}\text{H}_{11}\text{NO}_6\text{P}$, 296.0319; found, 296.0316.

Diethyl ((3-bromophenyl)difluoromethyl)phosphonate (7)

A suspended solution of Zn-dust (1.27 g, 19.4 mmol) in 3 mL DMF was purged with argon. To this solution diethyl (bromodifluoromethyl)phosphonate (3.4 mL, 19.4 mmol) in 2 mL DMF was added dropwise by maintaining reaction temperature at 50–60°C (rxn is exothermic). The reaction mixture was stirred at room temperature over 3 h and CuBr (2.79 g, 19.4 mmol) was added and stirred for 30 minutes at room temperature. A solution of bromo-3-iodobenzene (2.00 g, 7.1 mmol) in 1 mL DMF was added dropwise and was stirred for over 24 h at room temperature. Water (10 mL) and ether (10 mL) were added and mixture was passed through Celite. The layers were separated and aqueous layer was extracted by ether, organic extract was dried over MgSO_4 , filtered and solvent was removed. The crude material was purified via silica gel column chromatography (9:1 to 2:1 hexanes : EtOAc) to give pale yellow oil product (2.3 g, 96%). ^1H NMR (400 MHz, CDCl_3): δ 7.71 (s, 1H), 7.58 (m, 1H), 7.52 (m, 1H), 7.29 (m, 1H), 4.19 (m, 4H), 1.29 (m, 6H). ^{13}C NMR (400 MHz, CDCl_3): δ 133.86 (1C), 129.99 (1C), 129.97 (1C), 129.85 (1C), 129.25 (1C), 129.97 (1C), 122.40 (1C), 64.92 (1C), 64.85 (1C), 16.29 (1C), 16.24 (1C). APCI-MS (m/z): Calcd. for $\text{C}_{11}\text{H}_{14}\text{BrF}_2\text{O}_3\text{P}$, 342.0 and 344.0; Found, 343.0 and 345.0 $[\text{M} + \text{H}]^+$.

Diethyl (Difluoro(4'-(hydroxymethyl)-[1,1'-biphenyl]-3-yl)methyl)phosphonate (8)

Mixture of **7** (500.0 mg, 1.46 mmol), (4-(hydroxymethyl)phenyl)boronic acid (332.0 mg, 2.19 mmol) and $\text{Pd}(\text{PPh}_3)$ (84.0 mg, 0.07 mmol) in 5 mL saturated solution of K_2CO_3 , 2 mL EtOH and 5 mL toluene was purged with argon and stirred at 70° C overnight. Water (20 mL) was added upon cooling. The aqueous layer was extracted by EtOAc, and organic extract was dried over MgSO_4 , filtered and solvent was removed under reduced pressure.

Crude material was purified via silica gel chromatography (1.5:1 to 1:3 hexanes : EtOAc) to give a colorless oil product **8** as a yellow oil (308 mg, 57% yield). ¹H NMR (400 MHz, CDCl₃): δ 7.83 (m, 1H), 7.79 (m, 1H), 7.58 (m, 3H), 7.52 (m, 1H), 7.43 (m, 2H), 4.71 (s, 2H), 4.21 (m, 4H), 2.42 (s, 1H), 1.31 (m, 6H). ¹³C NMR (400 MHz, CDCl₃): δ 141.15 (1C), 140.78 (1C), 139.12 (1C), 133.11 (1C), 132.98 (1C), 129.36 (1C), 128.90 (1C), 127.40 (2C), 127.16 (2C), 124.95 (1C), 124.73 (1C), 64.90 (1C), 64.83 (1C), 16.31 (1C), 16.26 (1C). ESI-MS (*m/z*): Calcd. for C₁₈H₂₁F₂O₄P, 370.11; Found, 393.20 [M + Na]⁺.

Diethyl ((4'-((Aminoxy)methyl)-[1,1'-biphenyl]-3-yl)difluoromethyl)phosphonate (**9**)

To a mixture of **8** (184.0 mg, 0.50 mmol), *N*-hydroxyphthalimide (98.1 mg, 0.60 mmol), and PPh₃ (170.2 mg, 0.65 mmol) in anhydrous THF (5 mL) was added diisopropyl azodicarboxylate (DIAD) (0.13 mL, 0.65 mmol) and the mixture was stirred at room temperature overnight. The reaction mixture was partitioned (H₂O : EtOAc) and the organic layer was dried and taken to dryness. To a solution of the resultant product (168 mg, 0.33 mmol) in CH₂Cl₂ (5 mL) ethanol was added 50% aqueous hydrazine•hydrate (80 μL, 1.30 mmol) and the mixture was stirred at room temperature for 4 h. The resulting precipitate was removed by filtration and solvent was removed from the filtrate. The crude product was purified by silica column chromatography (50% to 100% EtOAc in hexanes) to yield **9** as an amorphous white solid (100 mg, 79% yield). ¹H NMR (400 MHz, CD₃OD): δ 7.81 (m, 2H), 7.59 (m, 4H), 7.46 (m, 2H), 4.73 (s, 2H), 4.20 (m, 4H), 1.30 (m, 6H). ¹³C NMR (400 MHz, CD₃OD): δ 141.17 (1C), 139.31 (1C), 137.26 (1C), 132.90 (1C), 132.76 (1C), 129.29 (1C), 129.27 (1C), 128.63 (2C), 128.23 (1C), 126.64 (2C), 124.63 (1C), 124.24 (1C), 76.98 (1C), 65.14 (1C), 65.07 (1C), 15.27 (1C), 15.21 (1C). APCI-MS (*m/z*): Calcd. for C₁₈H₂₂F₂NO₄P, 385.13; Found, 386.10 [M + H]⁺.

((4'-((Aminoxy)methyl)-[1,1'-biphenyl]-3-yl)difluoromethyl)phosphonic Acid (**5**)

To a solution of **9** (100 mg, 0.26 mmol) in anhydrous CH₂Cl₂ (5 mL) under argon was added trimethylsilylbromide (0.13 mL, 0.93 mmol) and the mixture was stirred at room temperature for 3 h. Solvent was removed and HPLC purification was performed as described in the General Synthetic methods (retention time = 15.6 minutes) to provide **5** as an amorphous white solid (44.4 mg, 52% yield). Analytical HPLC gave 99% purity. ¹H NMR (400 MHz, DMSO-*d*₆): δ 7.69–7.73 (m, 2H), 7.56 (m, 2H), 7.49 (m, 2H), 7.36 (m, 2H), 4.70 (s, 2H). HRMS-ESI (*m/z*): [M + H]⁺ calcd for C₁₄H₁₅NO₄F₂P, 330.0701; found, 330.0694.

(E)-5-(((3'-(Difluoro(phosphono)methyl)-[1,1'-biphenyl]-4-yl)methoxy)imino)methyl)furan-2-carboxylic acid (**6e**)

To a solution of **5** (8.2 mg, 0.025 mmol) and 5-formylfuran-2-carboxylic acid (4.2 mg, 0.030 mmol) in 2 mL DMSO was added AcOH (2.9 μL, 0.050 mmol). The reaction mixture was agitated at room temperature overnight. Product was purified via HPLC with a retention time of 18.4 min to give white solid product (7.8 mg, 69%). ¹H NMR (400 MHz, CD₃OD): δ 8.07 (s, 1H), 7.77 (s, 1H), 7.67 (d, *J* = 7.2 Hz, 1H), 7.56–7.59 (m, 2H), 7.41–7.52 (m, 5H), 7.22, 7.16 (d, *J* = 3.6 Hz, 1H), 7.18, 6.76 (d, *J* = 3.6 Hz, 1H), 5.26, 5.17 (s, 2H). ¹³C NMR (400 MHz, CDCl₃): δ 159.78 (1C), 150.55 (1C), 147.54 (1C), 145.59 (1C), 140.75 (1C), 139.89 (1C), 139.02 (1C), 136.89 (1C), 135.45 (1C), 128.55 (2C), 128.46 (1C), 128.44 (1C), 126.75 (1C), 126.66 (2C), 124.52 (1C), 118.78 (1C), 112.77 (1C), 76.01 (1C). HRMS-ESI (*m/z*): [M – H][–] calcd for C₂₀H₁₆F₂NO₇P, 450.0560; found, 450.0562.

Supplementary Material

Refer to Web version on PubMed Central for supplementary material.

Acknowledgments

Appreciation is expressed to Afroz Sultana (LMI) for technical support and to Joseph Tropea and Scott Cherry (MCL) for assistance with the production of phosphatases. Electrospray mass spectrometry experiments were conducted on the LC/ESMS instrument maintained by the Biophysics Resource in the Structural Biophysics Laboratory, Center for Cancer Research, National Cancer Institute at Frederick. X-ray diffraction data were collected at the Southeast Regional Collaborative Access Team (SER-CAT) beamline 22-ID at the Advanced Photon Source, Argonne National Laboratory. Supporting institutions may be found at <http://www.ser-cat.org/members.html>. Use of the Advanced Photon Source was supported by the U.S. Department of Energy, Office of Science, Office of Basic Energy Sciences, under contract no. W-31-109-Eng-38. This work was supported in part by the Intramural Research Program of the NIH, Center for Cancer Research, NCI-Frederick and the National Cancer Institute, National Institutes of Health and the Joint Science and Technology Office of the Department of Defense. The content of this publication does not necessarily reflect the views or policies of the Department of Health and Human Services, nor does mention of trade names, commercial products, or organizations imply endorsement by the U.S. Government.

References and Notes

1. Soulsby M, Bennett AM. Physiological signaling specificity by protein tyrosine phosphatases. *Physiology* (Bethesda). 2009; 24:281–289. [PubMed: 19815854]
2. Hunter T. Tyrosine phosphorylation: thirty years and counting. *Curr Opin Cell Biol*. 2009; 21:140–146. [PubMed: 19269802]
3. Zhang ZY, Lee SY. PTP1B inhibitors as potential therapeutics in the treatment of Type 2 diabetes and obesity. *Exp Opin Invest Drugs*. 2003; 12:223–233.
4. Ostman A, Hellberg C, Bohmer FD. Protein-tyrosine phosphatases and cancer. *Nat Rev Canc*. 2006; 6:307–320.
5. Jiang ZX, Zhang ZY. Targeting PTPs with small molecule inhibitors in cancer treatment. *Cancer Metastasis Rev*. 2008; 27:263–272. [PubMed: 18259840]
6. Vidovic D, Schurer SC. Knowledge-based characterization of similarity relationships in the human protein-tyrosine phosphatase family for rational inhibitor design. *J Med Chem*. 2009; 52:6649–6659. [PubMed: 19810703]
7. Titball RW, Leary SE. Plague. *Br Med Bull*. 1998; 54:625–633. [PubMed: 10326289]
8. Zhang ZY, Clemens JC, Schubert HL, Stuckey JA, Fischer MW, Hume DM, Saper MA, Dixon JE. Expression, purification, and physicochemical characterization of a recombinant *Yersinia* protein tyrosine phosphatase. *J Biol Chem*. 1992; 267:23759–23766. [PubMed: 1429715]
9. McGovern SL, Caselli E, Grigorieff N, Shoichet BK. A common mechanism underlying promiscuous inhibitors from virtual and high-throughput screening. *J Med Chem*. 2002; 45:1712–1722. [PubMed: 11931626]
10. McGovern SL, Helfand BT, Feng B, Shoichet BK. A specific mechanism of nonspecific inhibition. *J Med Chem*. 2003; 46:4265–4272. [PubMed: 13678405]
11. Seidler J, McGovern SL, Doman TN, Shoichet BK. Identification and prediction of promiscuous aggregating inhibitors among known drugs. *J Med Chem*. 2003; 46:4477–4486. [PubMed: 14521410]
12. Zhang ZY. Kinetic and mechanistic characterization of a mammalian protein-tyrosine phosphatase, PTP1. *J Biol Chem*. 1995; 270:11199–11204. [PubMed: 7744751]
13. Montserat J, Chen L, Lawrence DS, Zhang ZY. Potent low molecular weight substrates for protein-tyrosine phosphatase. *J Biol Chem*. 1996; 271:7868–7872. [PubMed: 8631832]
14. Chen L, Montserat J, Lawrence DS, Zhang ZY. VHR and PTP1 protein phosphatases exhibit remarkably different active site specificities toward low molecular weight nonpeptidic substrates. *Biochemistry*. 1996; 35:9349–9354. [PubMed: 8755712]
15. Taylor SD, Kotoris CC, Dinaut AN, Wang Q, Ramachandran C, Huang Z. Potent non-peptidyl inhibitors of protein tyrosine phosphatase 1B. *Bioor Med Chem*. 1998; 6:1457–1468.
16. Wood WJL, Patterson AW, Tsuruoka H, Jain RK, Ellman JA. Substrate activity screening: a fragment-based method for the rapid identification of nonpeptidic protease inhibitors. *J Am Chem Soc*. 2005; 127:15521–15527. [PubMed: 16262416]

17. Salisbury CM, Ellman JA. Rapid identification of potent nonpeptidic serine protease inhibitors. *ChemBioChem*. 2006; 7:1034–1037. [PubMed: 16708409]
18. Patterson AW, Wood WJL, Ellman JA. Substrate activity screening (SAS): a general procedure for the preparation and screening of a fragment-based non-peptidic protease substrate library for inhibitor discovery. *Nat Protoc*. 2007; 2:424–433. [PubMed: 17406604]
19. Inagaki H, Tsuruoka H, Hornsby M, Lesley SA, Spraggon G, Ellman JA. Characterization and optimization of selective, nonpeptidic inhibitors of cathepsin S with an unprecedented binding mode. *J Med Chem*. 2007; 50:2693–2699. [PubMed: 17469812]
20. Brak K, Doyle PS, McKerrow JH, Ellman JA. Identification of a new class of nonpeptidic inhibitors of cruzain. *J Am Chem Soc*. 2008; 130:6404–6410. [PubMed: 18435536]
21. Soellner MB, Rawls KA, Grundner C, Alber T, Ellman JA. Fragment-based substrate activity screening method for the identification of potent inhibitors of the *Mycobacterium tuberculosis* phosphatase PTPB. *J Am Chem Soc*. 2007; 129:9613–9615. [PubMed: 17636914]
22. Jenkins WT, Marshall MM. A modified direct phosphate assay for studying ATPases. *Anal Biochem*. 1984; 141:155–160. [PubMed: 6238550]
23. Black MJ, Jones ME. Inorganic phosphate determination in the presence of a labile organic phosphate: Assay for carbamyl phosphate phosphatase activity. *Anal Biochem*. 1983; 135:233–238. [PubMed: 6322612]
24. Webb MR. A continuous spectrophotometric assay for inorganic phosphate and for measuring phosphate release kinetics in biological systems. *Proc Nat Acad Sci USA*. 1992; 89:4884–487. [PubMed: 1534409]
25. Tautz L, Mustelin T. Strategies for developing protein tyrosine phosphatase inhibitors. *Methods*. 2007; 42:250–260. [PubMed: 17532512]
26. Zhang ZY. Pre-steady-state and steady-state kinetic analysis of the low molecular weight phosphotyrosyl protein phosphatase from bovine heart. *J Biol Chem*. 1991; 266:1516–1525. [PubMed: 1703150]
27. Puius YA, Zhao Y, Sullivan M, Lawrence DS, Almo SC, Zhang ZY. Identification of a second aryl phosphate-binding site in protein-tyrosine phosphatase 1B: a paradigm for inhibitor design. *Proc Nat Acad Sci USA*. 1997; 94:13420–13425. [PubMed: 9391040]
28. Guo XL, Shen K, Wang F, Lawrence DS, Zhang ZY. Probing the molecular basis for potent and selective protein-tyrosine phosphatase 1B inhibition. *J Biol Chem*. 2002; 277:41014–41022. [PubMed: 12193602]
29. Chen YT, Seto CT. Divalent and trivalent alpha-ketocarboxylic acids as inhibitors of protein tyrosine phosphatases. *J Med Chem*. 2002; 45:3946–3952. [PubMed: 12190316]
30. Chen YT, Seto CT. Parallel synthesis of a library of bidentate protein tyrosine phosphatase inhibitors based on the alpha-ketoacid motif. *Bioorg Med Chem*. 2004; 12:3289–3298.
31. Xie J, Seto CT. Investigations of linker structure on the potency of a series of bidentate protein tyrosine phosphatase inhibitors. *Bioorg Med Chem*. 2005; 13:2981–2991. [PubMed: 15781408]
32. Liu G, Xin Z, Pei Z, Hajduk PJ, Abad-Zapatero C, Hutchins CW, Zhao H, Lubben TH, Ballaron SJ, Haasch DL, Kaszubska W, Rondinone CM, Trevillyan JM, Jirousek MR. Fragment screening and assembly: A highly efficient approach to a selective and cell active protein tyrosine phosphatase 1B inhibitor. *J Med Chem*. 2003; 46:4232–4235. [PubMed: 13678400]
33. Comeau AB, Critton DA, Page R, Seto CT. A focused library of protein tyrosine phosphatase inhibitors. *J Med Chem*. 2010; 53:6768–6772. [PubMed: 20731359]
34. Kolb HC, Finn MG, Sharpless KB. Click chemistry: Diverse chemical function from a few good reactions. *Angewandte Chem Int Ed Engl*. 2001; 40:2004–2021.
35. Liu F, Stephen AG, Fisher RJ, Burke TR Jr. Protected aminooxyprolines for expedited library synthesis: Application to Tsg101-directed proline-oxime containing peptides. *Bioorg Med Chem Lett*. 2008; 18:1096–1101. [PubMed: 18083557]
36. Liu F, Stephen AG, Waheed AA, Aman MJ, Freed EO, Fisher RJ, Burke TR Jr. SAR by oxime-containing peptide libraries: application to Tsg101 ligand optimization. *ChemBiochem*. 2008; 9:2000–2004. [PubMed: 18655064]

37. Liu F, Thomas J, Burke TR Jr. Synthesis of a homologous series of side-chain-extended orthogonally protected aminoxy-containing amino acids. *Synthesis*. 2008;2432–2438. [PubMed: 19122755]
38. Liu F, Hakami RM, Dyas B, Bahta M, Lountos GT, Waugh DS, Ulrich RG, Burke TR Jr. A rapid oxime linker-based library approach to identification of bivalent inhibitors of the *Yersinia pestis* protein-tyrosine phosphatase, YopH. *Bioor Med Chem Lett*. 2010; 20:2813–2816.
39. Maly DJ, Choong IC, Ellman JA. Combinatorial target-guided ligand assembly: Identification of potent subtype-selective c-Src inhibitors. *Proc Natl Acad Sci US A*. 2000; 97:2419–2424.
40. Jiang YL, Krosky DJ, Seiple L, Stivers JT. Uracil-directed ligand tethering: An efficient strategy for uracil DNA glycosylase (UNG) inhibitor development. *J Am Chem Soc*. 2005; 127:17412–17420. [PubMed: 16332091]
41. Johnson SM, Petrassi HM, Palaninathan SK, Mohamedmohaideen NN, Purkey HE, Nichols C, Chiang KP, Walkup T, Sacchettini JC, Sharpless KB, Kelly JW. Bisaryloxime ethers as potent inhibitors of transthyretin amyloid fibril formation. *J Med Chem*. 2005; 48:1576–1587. [PubMed: 15743199]
42. Chung S, Parker JB, Bianchet M, Amzel LM, Stivers JT. Impact of linker strain and flexibility in the design of a fragment-based inhibitor. *Nat Chem Biol*. 2009; 5:407–413. [PubMed: 19396178]
43. Srinivasan R, Uttamchandani M, Yao SQ. Rapid assembly and in situ screening of bidentate inhibitors of protein tyrosine phosphatases. *Org Lett*. 2006; 8:713–716. [PubMed: 16468749]
44. Tan LP, Wu H, Yang PY, Kalesh KA, Zhang X, Hu M, Srinivasan R, Yao SQ. High-throughput discovery of *Mycobacterium tuberculosis* protein tyrosine phosphatase B (MptpB) inhibitors using click chemistry. *Org Lett*. 2009; 11:5102–5105. [PubMed: 19852491]
45. Zhou B, He Y, Zhang X, Xu J, Luo Y, Wang Y, Franzblau SG, Yang Z, Chan RJ, Liu Y, Zheng J, Zhang ZY. Targeting mycobacterium protein tyrosine phosphatase B for antituberculosis agents. *Proc Natl Acad Sci U S A*. 2010; 107:4573–4578. [PubMed: 20167798]
46. Srinivasan R, Tan LP, Wu H, Yang PY, Kalesh KA, Yao SQ. High-throughput synthesis of azide libraries suitable for direct “click” chemistry and in situ screening. *Org Biomol Chem*. 2009; 7:1821–1828. [PubMed: 19590777]
47. Smyth MS, Ford H Jr, Burke TR Jr. A general method for the preparation of benzylic alpha, alpha-difluorophosphonic acids; non-hydrolyzable mimetics of phosphotyrosine. *Tetrahedron Lett*. 1992; 33:4137–4140.
48. Burke TR Jr, Kole HK, Roller PP. Potent inhibition of insulin receptor dephosphorylation by a hexamer peptide containing the phosphotyrosyl mimetic F₂Pmp. *Biochem Biophys Res Commun*. 1994; 204:129–134. [PubMed: 7524496]
49. Yao ZJ, Ye B, Wu XW, Wang SM, Wu L, Zhang ZY, Burke TR Jr. Structure-based design and synthesis of small molecule protein-tyrosine phosphatase 1B inhibitors. *Bioorg Med Chem*. 1998; 6:1799–1810. [PubMed: 9839010]
50. Sun JP, Wu L, Fedorov AA, Almo SC, Zhang ZY. Crystal structure of the *Yersinia* protein-tyrosine phosphatase YopH complexed with a specific small molecule inhibitor. *J Biol Chem*. 2003; 278:33392–33399. [PubMed: 12810712]
51. Yokomatsu T, Murano T, Suemune K, Shibuya S. Facile synthesis of aryl(difluoromethyl)phosphonates through CuBr-mediated cross coupling reactions of [(diethoxyphosphinyl)difluoromethyl]zinc bromide with aryl iodides. *Tetrahedron*. 1997; 53:815–822.
52. Li Z, Yeo SL, Pallen CJ, Ganesan A. Solid-phase synthesis of potential protein tyrosine phosphatase inhibitors via the Ugi four-component condensation. *Bioor Med Chem Lett*. 1998; 8:2443–2446.
53. Phan J, Lee K, Cherry S, Tropea JE, Burke TR Jr, Waugh DS. High-resolution structure of the *Yersinia pestis* protein tyrosine phosphatase YopH in complex with a phosphotyrosyl mimetic-containing hexapeptide. *Biochemistry*. 2003; 42:13113–13121. [PubMed: 14609321]
54. Kolmodin K, Aqvist J. The catalytic mechanism of protein tyrosine phosphatases revisited. *FEBS Lett*. 2001; 498:208–213. [PubMed: 11412859]
55. Denu JM, Dixon JE. Protein tyrosine phosphatases: mechanisms of catalysis and regulation. *Curr Opin Chem Biol*. 1998; 2:633–641. [PubMed: 9818190]

56. Zhang ZY. Protein-tyrosine phosphatases: biological function, structural characteristics, and mechanism of catalysis. *Crit Rev Biochem Mol Biol*. 1998; 33:1–52. [PubMed: 9543627]
57. ICM Chemist Pro Software v 3.7-1f/MacOSX. MolSoft LLC; La Jolla, CA: [https://www.molsoft.com/icm-chemist-pro.html]
58. Abagyan, R.; Orry, A.; Raush, E.; Totrov, M. ICM User Guide 3.6. MolSoft LLC; La Jolla, CA: [https://www.molsoft.com/icm/index.html]
59. Zhang S, Zhang ZY. PTP1B as a drug target: recent developments in PTP1B inhibitor discovery. *Drug Discov Today*. 2007; 12:373–381. [PubMed: 17467573]
60. Tautz L, Bruckner S, Sareth S, Alonso A, Bogetz J, Bottini N, Pellecchia M, Mustelin T. Inhibition of *Yersinia* tyrosine phosphatase by furanyl salicylate compounds. *J Biol Chem*. 2005; 280:9400–9408. [PubMed: 15615724]
61. Feng BY, Shelat A, Doman TN, Guy RK, Shoichet BK. High-throughput assays for promiscuous inhibitors. *Nat Chem Biol*. 2005; 1:146–148. [PubMed: 16408018]
62. Ryan AJ, Gray NM, Lowe PN, Chung CW. Effect of detergent on “promiscuous” inhibitors. *J Med Chem*. 2003; 46:3448–3451. [PubMed: 12877581]
63. Streuli M, Krueger NX, Hall LR, Schlossman SF, Saito H. A new member of the immunoglobulin superfamily that has a cytoplasmic region homologous to the leukocyte common antigen. *J Exp Med*. 1988; 168:1523–1530. [PubMed: 2972792]
64. Patterson KI, Brummer T, O’Brien PM, Daly RJ. Dual-specificity phosphatases: critical regulators with diverse cellular targets. *Biochem J*. 2009; 418:475–489. [PubMed: 19228121]
65. Saikh KU, Khan AS, Kissner T, Ulrich RG. IL-15-induced conversion of monocytes to mature dendritic cells. *Clin Exp Immunol*. 2001; 126:447–455. [PubMed: 11737061]
66. Tangy F, Moukkadem M, Vindimian E, Capmau ML, Le Goffic F. Mechanism of action of gentamicin components. Characteristics of their binding to *Escherichia coli* ribosomes. *Eur J Biochem*. 1985; 147:381–386. [PubMed: 3882427]
67. Tropea JE, Phan J, Waugh DS. Overproduction, purification, and biochemical characterization of the dual specificity H1 protein phosphatase encoded by Variola major virus. *Prot Exp Purif*. 2006; 50:31–36.
68. Lountos GT, Tropea JE, Cherry S, Waugh DS. Overproduction, purification and structure determination of human dual-specificity phosphatase 14. *Acta Crystallogr Section D*. 2009; 65:1013–1020.
69. Tropea, JE.; Cherry, S.; Nallamsetty, S.; Bignon, C.; Waugh, DS. A generic method for the production of recombinant proteins in *Escherichia coli* using a dual hexahistidine-maltose-binding protein affinity tag. In: Doublet, S., editor. *Meth Mol Biol*. Humana Press, Inc; Totowa, NJ: 2007. p. 1-19. (Macromol. Crystall. Protocols: Vol 1: Preparation and Crystallization of Macromolecules)
70. Welkos S, Pitt ML, Martinez M, Friedlander A, Vogel P, Tammariello R. Determination of the virulence of the pigmentation-deficient and pigmentation-/plasminogen activator-deficient strains of *Yersinia pestis* in non-human primate and mouse models of pneumonic plague. *Vaccine*. 2002; 20:2206–2214. [PubMed: 12009274]
71. Minor W, Cymborowski M, Otwinowski Z, Chruszcz M. HKL-3000: the integration of data reduction and structure solution—from diffraction images to an initial model in minutes. *Acta Crystallogr D Biol Crystallogr*. 2006; 62:859–866. [PubMed: 16855301]
72. Vagin A, Teplyakov A. Molecular replacement with MOLREP. *Acta Crystallogr D Biol Crystallogr*. 2010; 66:22–25. [PubMed: 20057045]
73. The CCP4 suite: programs for protein crystallography. *Acta Crystallogr D Biol Crystallogr*. 1994; 50:760–763. [PubMed: 15299374]
74. Murshudov GN, Vagin AA, Dodson EJ. Refinement of macromolecular structures by the maximum-likelihood method. *Acta Crystallogr D Biol Crystallogr*. 1997; 53:240–255. [PubMed: 15299926]
75. Emsley P, Cowtan K. Coot: model-building tools for molecular graphics. *Acta Crystallogr D Biol Crystallogr*. 2004; 60:2126–2132. [PubMed: 15572765]
76. Read RJ. Model phases: probabilities and bias. *Meth Enzym*. 1997; 277:110–128. [PubMed: 18488308]

77. Schuttelkopf AW, van Aalten DM. PRODRG: a tool for high-throughput crystallography of protein-ligand complexes. *Acta Crystallogr D Biol Crystallogr*. 2004; 60:1355–1363. [PubMed: 15272157]
78. Brunger AT. Free R value: a novel statistical quantity for assessing the accuracy of crystal structures. *Nature*. 1992; 355:472–475. [PubMed: 18481394]
79. Davis IW, Leaver-Fay A, Chen VB, Block JN, Kapral GJ, Wang X, Murray LW, Arendall WB 3rd, Snoeyink J, Richardson JS, Richardson DC. MolProbity: all-atom contacts and structure validation for proteins and nucleic acids. *Nucleic Acids Res*. 2007; 35:W375–383. [PubMed: 17452350]

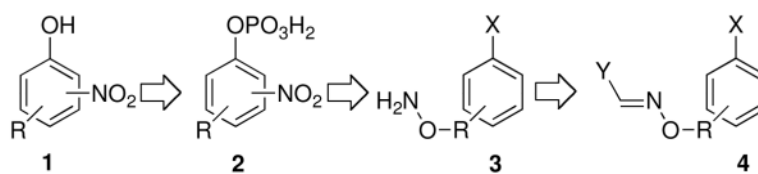


Figure 1. Design progression leading from a library of nitrophenylphosphates (**1**) to bidentate inhibitors (**4**).

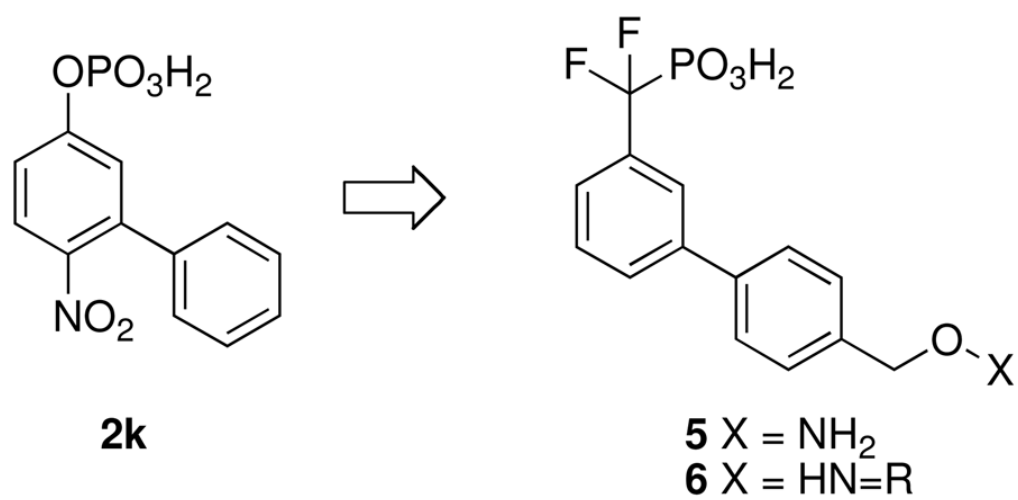


Figure 2.
Development of oxime-containing inhibitors (**6**) starting from platform **2k**.

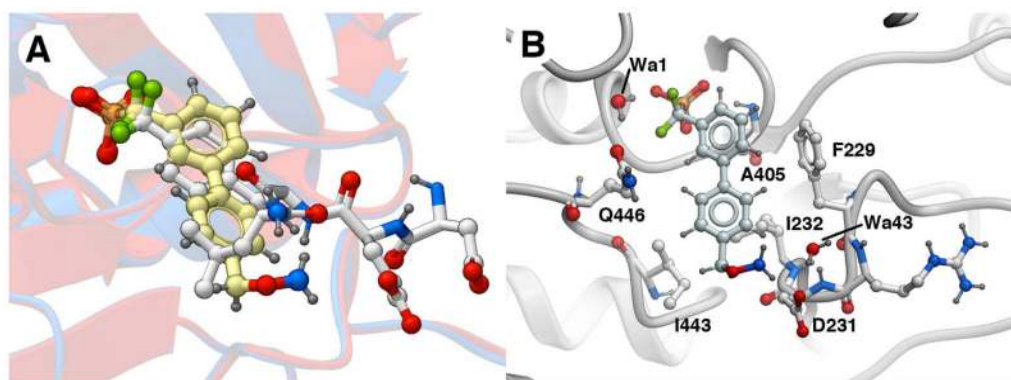


Figure 3. Crystal structures of YopH-bound ligands. (A) Superposition of the complex YopH•[Ac-Asp-Ala-Asp-Glu-F₂Pmp-Leu-amide] (protein backbone in red, ligand carbons in white; PDB code 1QZ0) with YopH•**5** (protein backbone in blue, ligand carbons in yellow) showing relative binding orientations of the two ligands. (B) Residues providing key hydrophobic contacts with **5**.

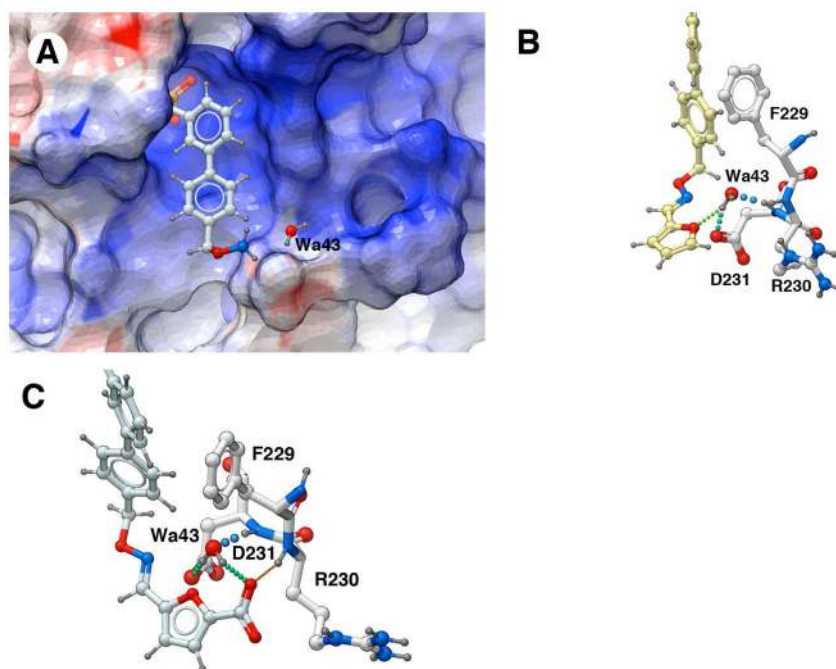


Figure 4. Role of conserved water (Wa43) in the design of inhibitor **6e**. (A) Electrostatic potential surface rendering (blue = positive; red = negative) of the YopH•5 complex highlighting a key conserved water (Wa43). (B) Predicted interaction of the furanyloxime oxygen of **6b** with Wa43. (C) Predicted interaction of the 5-carboxyfuranyloxime group of **6e** with Wa43 and the protein backbone.

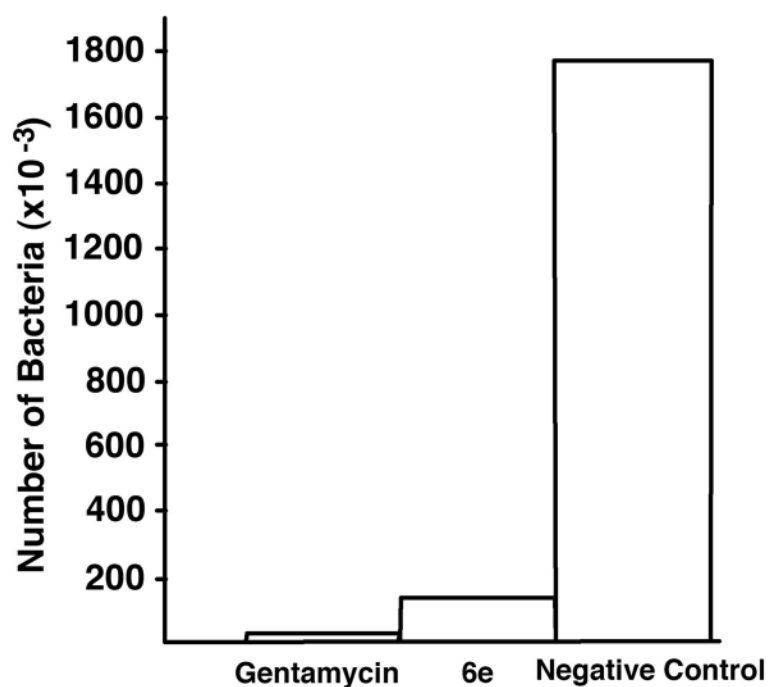
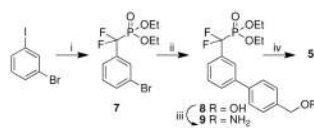


Figure 5. Effect of compounds on intracellular replication of *Y. pestis*. Primary human monocytes were infected with *Y. pestis* and cultured 12 h with **6e** or a negative control (10 μ M each). Gentamycin was included as a positive control. Results are presented as viable intracellular bacteria recovered per well of monocytes. Standard errors of the mean were <10%. The assay was performed on three separate occasions using three independent monocyte donors.

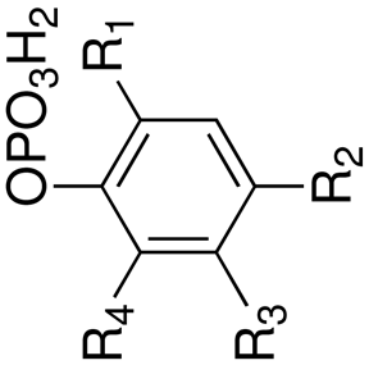


Scheme 1.

Synthesis of inhibitor platform **5**. Reagents and conditions: (i) Zn, diethyl (bromodifluoromethyl)phosphonate, CuBr, DMF, 60° C to room temperature (96% yield); (ii) 4-(hydroxymethyl)phenylboronic acid, Pd(PPh₃)₄, satd. K₂CO₃, EtOH, PhMe, 70° C (45% yield); (iii) a) *N*-hydroxyphthalimide, PPh₃, DIAD, THF, room temperature b) NH₂NH₂•H₂O, EtOH, room temp. (75% yield); (iv) TMSBr, CH₂Cl₂, room temperature (72% yield).

Table 1

In vitro YopH K_M values for selected substrates.



Substrate	R ¹	R ²	R ³	R ⁴	$K_M \pm \text{S.E. (mM)}^a$
<i>p</i> NPP	H	NO ₂	H	H	0.60 ± 0.10
2a	NO ₂	<i>t</i> -Bu	H	H	0.47 ± 0.06
2b	H	NO ₂	<i>t</i> -Bu	H	1.14 ± 0.19
2c	NO ₂	-CH ₂ ONH ₂	H	H	1.13 ± 0.15
2d	H	NO ₂	-CH ₂ ONH ₂	H	0.41 ± 0.05
2e	H	NO ₂	CH ₂ ON=CHMe	H	0.17 ± 0.02
2f	H	NO ₂	H	Me	0.65 ± 0.11
2g	NO ₂	H	H	Me	No activity
2h	Cyclohexyl	NO ₂	H	H	0.26 ± 0.02
2i	NO ₂	H	H	Cyclohexyl	No activity
2j	NO ₂	Ph	H	H	0.15 ± 0.03
2k	H	NO ₂	Ph	-H	0.08 ± 0.01

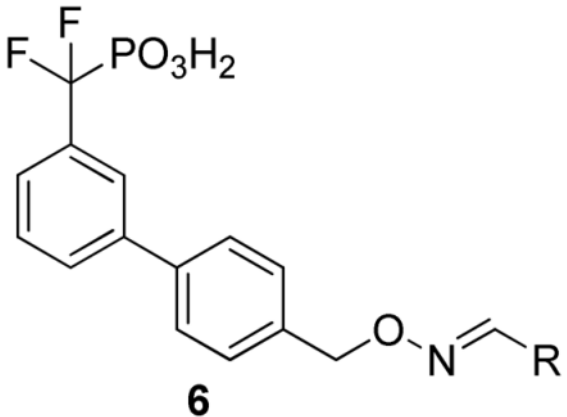
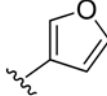
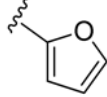
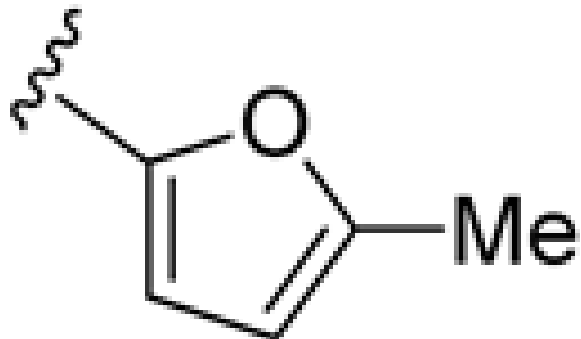
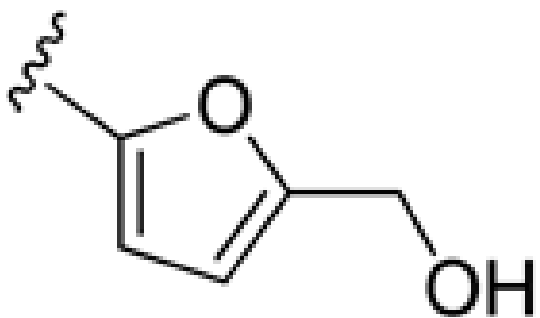
^a K_M values were determined as indicated in the Experimental Procedures.

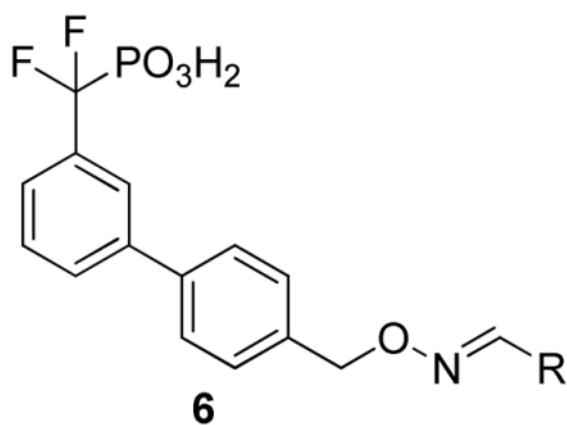
Table 2Comparison of YopH hydrophobic contact residues for compound 5 and F₂Pmp-Leu.

Residue	5 ^a	F ₂ Pmp-Leu ^{a, b}
F229	24.6	24.6
D231	24.1	30.2
I232	23.6	19.8
A405	23.0	24.1
Q446	21.1	29.1
I443	11.0	16.0

^aContact is given in Å²;^bData for F₂Pmp-Leu was derived from PDB Code 1QZ0.

Table 3*In vitro* YopH IC₅₀ values for selected inhibitors.

 6		
No.	R	IC ₅₀ ± S.E. (μM) ^a
6a		3.69 ± 0.31
6b		1.20 ± 0.22
6c		0.91 ± 0.13
6d		0.73 ± 0.30



No.	R	IC ₅₀ ± S.E. (μM) ^a
6e		0.19 ± 0.16

^aIC₅₀ values were determined as indicated in the Experimental Procedures.

Table 4Inhibitory potencies of **6e** against a panel of phosphatases.^a

Phosphatase	IC ₅₀ (μM)	Fold Difference
YopH	0.19	Reference Value
PTP1B	2.23	11.7
LAR	> 400	> 2000
DUS P-14	> 400	> 2000
DUS P-22	> 400	> 2000
VH1	> 400	> 2000

^aValues were determined as described in the Experimental Procedures.

Table 5

Data collection and refinement statistics.

Data collection	
X-ray source	22-ID, SER-CAT
Wavelength (Å)	1.0
Resolution (Å)	50.0–1.78 (1.80–1.78) ^a
Space group	P 2 ₁ 2 ₁ 2 ₁
Unit cell dimensions (°)	<i>a</i> =49.2, <i>b</i> =55.5, <i>c</i> =100.1
Total Reflections/unique reflections	148922/25241
Completeness (%)	92.8/74.8
<i>R</i> _{sym} (%) ^b	10.6 (49.8)
<i>I</i> /σ(<i>I</i>)	21.9 (2.3)
Redundancy	5.9 (4.1)
Refinement statistics	
Resolution (Å)	50.0–1.78
No. of reflections working set/test set	23875/25241
<i>R</i> -work (%)	16.5
<i>R</i> -free (%)	21.0
No. of atoms/mean <i>B</i> -factor (Å ²)	
Protein	2237/15.5
Inhibitor	22/15.7
Water	274/29.3
r.m.s. deviation from ideal geometry	
Bond lengths (Å)/bond angles (°)	0.014/1.5
Ramachandran plot	
Most favored (%)	93.2
Additionally allowed (%)	6.4
Generously allowed (%)	0.4
Disallowed (%)	0
MolProbity protein geometry score	1.53 (92 nd percentile)
PDB accession code	2Y2F

^aValues in parenthesis are for reflections in the highest resolution shell.

^b $R_{\text{sym}} = \frac{\sum_{hkl} \sum_i |I_i(hkl) - \langle I(hkl) \rangle|}{\sum_{hkl} \sum_i I_i(hkl)}$, where $\langle I(hkl) \rangle$ is the mean intensity of multiply recorded reflections.

^c $R = \frac{\sum |F_{\text{obs}}(hkl) - F_{\text{calc}}(hkl)|}{\sum |F_{\text{obs}}(hkl)|}$. *R*_{free} is the *R* value calculated for 5% of the data set not included in the refinement.